Josephson parametric phase-locked oscillator and its application to dispersive readout of superconducting qubits

Z.R. Lin[1], K. Inomata[1], K. Koshino[2], W.D. Oliver[3], Y. Nakamura[1,4], J.S. Tsai[1,5] & T. Yamamoto[1,5]

The parametric phase-locked oscillator (PPLO) is a class of frequency-conversion device, originally based on a nonlinear element such as a ferrite ring, that served as a fundamental logic element for digital computers more than 50 years ago. Although it has long since been overtaken by the transistor, there have been numerous efforts more recently to realize PPLOs in different physical systems such as optical photons, trapped atoms, and electromechanical resonators. This renewed interest is based not only on the fundamental physics of nonlinear systems, but also on the realization of new, high-performance computing devices with unprecedented capabilities. Here we realize a PPLO with Josephson-junction circuitry and operate it as a sensitive phase detector. Using a PPLO, we demonstrate the demodulation of a weak binary phase-shift keying microwave signal of the order of a femtowatt. We apply PPLO to dispersive readout of a superconducting qubit, and achieved high-fidelity, single-shot and non-destructive readout with Rabi-oscillation contrast exceeding 90%.

[1] Center for Emergent Matter Science (CEMS), RIKEN, Wako, Saitama 351-0198, Japan. [2] College of Liberal Arts and Sciences, Tokyo Medical and Dental University, Ichikawa, Chiba 272-0827, Japan. [3] Lincoln Laboratory, Massachusetts Institute of Technology, Lexington, Massachusetts 02420, USA. [4] Research Center for Advanced Science and Technology (RCAST), The University of Tokyo, Meguro-ku, Tokyo 153-8904, Japan. [5] Smart Energy Research Laboratories, NEC Corporation, Tsukuba, Ibaraki 305-8501, Japan. Correspondence and requests for materials should be addressed to T.Y. (email: t-yamamoto@fe.jp.nec.com).

The parametric phase-locked oscillator (PPLO)[1], also known as a parametron[2], is a resonant circuit in which one of the reactances is periodically modulated. It can detect, amplify, and store binary digital signals in the form of two distinct phases of self-oscillation. Indeed, digital computers using PPLOs based on a magnetic ferrite ring or a varactor diode as its fundamental logic element were successfully operated in 1950s and 1960s[2]. More recently, basic bit operations have been demonstrated in an electromechanical resonator[3], and an Ising machine based on optical PPLOs has been proposed[4]. PPLOs also offer an interesting system to study fundamental physics of nonlinear oscillators[5]. Here using a PPLO realized with Josephson-junction circuitry, we demonstrate the demodulation of a microwave signal digitally modulated by binary phase-shift keying (BPSK). Moreover, we apply this demodulation capability to the dispersive readout of a superconducting qubit. This readout scheme enables a fast and latching-type readout, yet requires only a small number of readout photons in the resonator to which the qubit is coupled, thus featuring the combined advantages of several disparate schemes[6,7]. We have achieved high-fidelity, single-shot and non-destructive qubit readout with Rabi-oscillation contrast exceeding 90%, limited primarily by the qubit's energy relaxation.

Results

PPLO with Josephson-junction circuitry. Our PPLO is implemented by a superconducting coplanar waveguide (CPW) resonator defined by a coupling capacitor C_{in}^{PO} and a dc-SQUID (superconducting quantum interference device) termination (Fig. 1a; see Supplementary Fig. 1 and Supplementary Note 1 for the details of the device). The dc-SQUID, working as a controllable inductor, makes the resonant frequency of the resonator ω_0^{PO} dependent on an external magnetic flux through the SQUID loop Φ_{sq} (ref. 8). The application of a microwave field at a frequency ω_p and a power P_p to the pump line, which is inductively coupled to the SQUID loop, modulates the resonant frequency around its static value. This device has previously been operated as a Jopsehson parametric amplifier[9,10]. The signal at $\sim \omega_0^{PO}$ entering the resonator obtains a parametric gain produced by the pump at $\omega_p \sim 2\omega_0^{PO}$ and is reflected back along the signal line. This device also works as a parametric oscillator when it is operated at P_p above the threshold P_{p0} determined by the photon decay rate of the resonator[11,12]. Namely, it generates an output microwave field at $\omega_p/2$ even without any signal injection. The output can be one of the two degenerate oscillatory states (0π and 1π states) that differ solely by a relative phase shift π.

When an additional signal at $\sim \omega_p/2$ with a power P_s^{PO}, which we call the locking signal (LS), is injected into the parametric oscillator, the degeneracy of the two oscillatory states is lifted[13]. Such degeneracy lifting has been demonstrated in other physical systems such as magneto-optically trapped cold atoms[14] and electromechanical systems[15]. To understand the dynamics, we consider the Hamiltonian of the PPLO including a signal port for the LS and a fictitious loss port for internal loss of the resonator, namely,

$$\mathcal{H}/\hbar = \omega_0^{PO} a^\dagger a + \frac{\kappa}{2}\sqrt{\frac{P_p}{P_{p0}}}\cos(2\omega_0^{PO}t)\left(a + a^\dagger\right)^2 + \gamma\left(a + a^\dagger\right)^4$$
$$+ \int dk\left[v_b k b_k^\dagger b_k + i\sqrt{\frac{v_b \kappa_1}{2\pi}}\left(a^\dagger b_k - b_k^\dagger a\right)\right] \quad (1)$$
$$+ \int dk\left[v_c k c_k^\dagger c_k + i\sqrt{\frac{v_c \kappa_2}{2\pi}}\left(a^\dagger c_k - c_k^\dagger a\right)\right],$$

where γ represents the nonlinearity of the Josephson junction (JJ), a is the annihilation operator for the resonator, b_k (c_k) is the
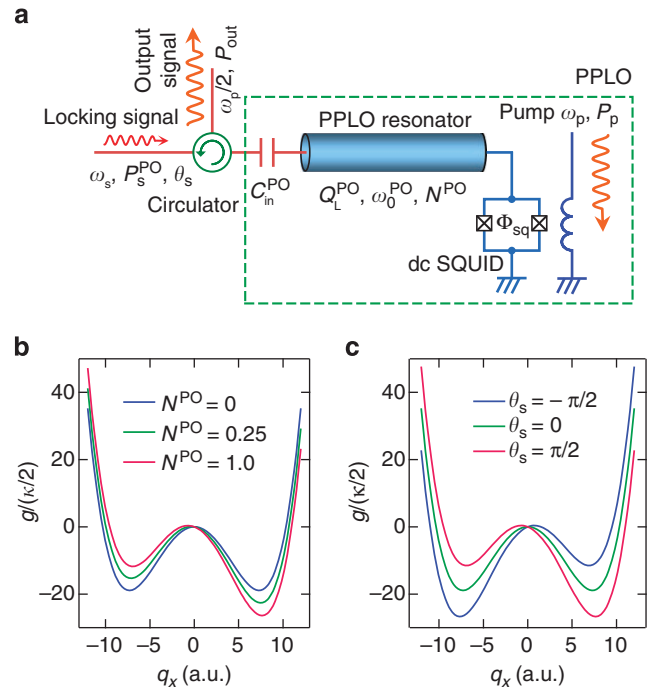
Figure 1 | Parametric phase-locked oscillator (PPLO). (a) Schematic of the device. The application of a pump microwave field at $\omega_p \sim 2\omega_0^{PO}$ with a power P_p above the threshold generates an output signal at $\omega_p/2$ with a power P_{out}. Here, ω_0^{PO} is the static resonant frequency of the PPLO resonator, and ω_s, P_s^{PO} and θ_s represent the frequency, power and phase of the LS, respectively. C_{in}^{PO} represents the coupling capacitance between the resonator and the feedline, and Φ_{sq} represents the magnetic flux penetrating the SQUID loop. **(b)** Cross-section of the Hamiltonian $g(q_x, 0)$ in the rotating frame for various powers and a fixed phase ($\theta_s = \pi/2$) of the LS. Here the LS power is represented by the mean photon number in the PPLO resonator, $N^{PO} = 4P_s^{PO} Q_L^{PO2}/\left(\hbar \omega_0^{PO2} Q_e^{PO}\right)$. Here the internal ($Q_i^{PO}$) and external ($Q_e^{PO}$) quality factors of the PPLO resonator are measured to be 5,200 and 340, respectively at $\omega_0^{PO}/2\pi = 10.507$ GHz, which give a loaded quality factor Q_L^{PO} of 320. The pump power P_p/P_{p0} is fixed at 2.0. Two minima correspond to 0π and 1π states of the phase-locked oscillations. **(c)** Same as **b**, but for $N^{PO} = 1$ and various values of θ_s.

annihilation operator for the photon in the signal (loss) port with a wave number k and a velocity v_b (v_c), κ_1 (κ_2) represents the coupling strength between the resonator and the signal (loss) port and $\kappa = \kappa_1 + \kappa_2$. The equations of motion for the classical resonator field in a frame rotating at ω_0^{PO} are obtained from the Hamiltonian by setting $\langle a\rangle = [q_x(t) - iq_y(t)]e^{-i\omega_0^{PO}t}$ and are given by (ref. 16; also see Supplementary Note 2 for derivation)

$$\frac{dq_x}{dt} = -\frac{\kappa}{2}q_x + \frac{\partial g}{\partial q_y}, \quad (2)$$

$$\frac{dq_y}{dt} = -\frac{\kappa}{2}q_y - \frac{\partial g}{\partial q_x}, \quad (3)$$

where

$$g(q_x, q_y) = \frac{\kappa}{4}\sqrt{\frac{P_p}{P_{p0}}}\left(q_y^2 - q_x^2\right) - 3\gamma\left(q_x^2 + q_y^2\right)^2$$
$$+ \sqrt{\kappa_1}|E_s|\left(q_y\cos\theta_s - q_x\sin\theta_s\right), \quad (4)$$

and $|E_s| = \sqrt{P_s^{PO}/\hbar\omega_0^{PO}}$ and θ_s are the amplitude and phase of the LS, respectively. In the absence of the first term (oscillator's

friction term) on the right-hand side, equations (2) and (3) are in the form of Hamilton's equations of motion with the Hamiltonian $g(q_x, q_y)$, whose minima correspond to 0π and 1π states[16]. As shown in Fig. 1b, $g(q_x, 0)$ is symmetric with respect to q_x when there is no LS ($|E_s| = 0$), and 0π and 1π states are degenerate. When we apply LS, it gives a tilt to the double well, which is proportional to $|E_s| \sin \theta_s$ (Fig. 1b,c). This lifts the degeneracy, and the PPLO, initially at $q_x, q_y \sim 0$, preferably evolves into one of the two states. This is how the amplitude and the phase of LS control the output state of the PPLO.

Output of PPLO. Now we show the experimental results. Figure 2a shows the output power of the PPLO operated at $\omega_p = 2\omega_0^{PO} = 2\pi \times 21.014$ GHz (solid blue circles) as a function of P_p in the absence of LS injection. For each P_p, the microwave field is continuously applied to the pump port and the output signal at $\omega_p/2$ is measured by a spectrum analyser. Note that power levels stated in this work are referred to the corresponding ports on the chip. The steep increase of the output power at $P_p \sim -65$ dBm indicates the onset of the parametric oscillation. This is further confirmed by detecting the response to the pulsed pump. Figure 2b shows the histogram of the demodulated amplitude and phase of the output signal plotted in the quadrature (IQ) plane. For each application of the pump pulse with an amplitude of $P_p = -62$ dBm, we recorded the output pulse and extracted its amplitude and phase by averaging for 100 ns. The two distribution peaks correspond to 0π and 1π states. They have equal amplitude but different phases shifted by π, and are observed with equal probabilities as expected.

Next we perform a similar measurement, but include LS injection. Figure 2c shows the histogram of the demodulated phase of the output signal as a function of the LS phase. While continuously injecting LS with a phase θ_s and a power $P_s^{PO} = -125$ dBm, we applied a pulsed pump with the same duration and the amplitude as in Fig. 2b, and extracted the phase of the output signal. As exemplified by the cross-section along the dashed line, the probabilities of obtaining the two states are no longer equal and depend on θ_s. In Fig. 2d, we plot the probability of 0π state as a function of θ_s for different P_s^{PO}s. The probability shows sinusoidal dependence when P_s^{PO} is small. As we increase P_s^{PO}, the modulation amplitude ($\Delta P_{0\pi}$) also increases and finally reaches unity. We define $(1 - \Delta P_{0\pi})/2$ as a non-locking error and plot it as a function of P_s^{PO} in Fig. 2e using blue circles. When P_s^{PO} is larger than ~ -125 dBm (corresponding to N^{PO} of 0.9), the non-locking error becomes negligible. We also simulated the non-locking error by solving a master equation[17] based on the Hamiltonian (equation (1)) and plot it by red curve (for details, see Supplementary Note 2 and Supplementary Figs 2 and 3). The only assumption here is the pump threshold P_{p0}, which is set to be -64.0 dBm. The agreement between the theory and the experiment is fairly good.
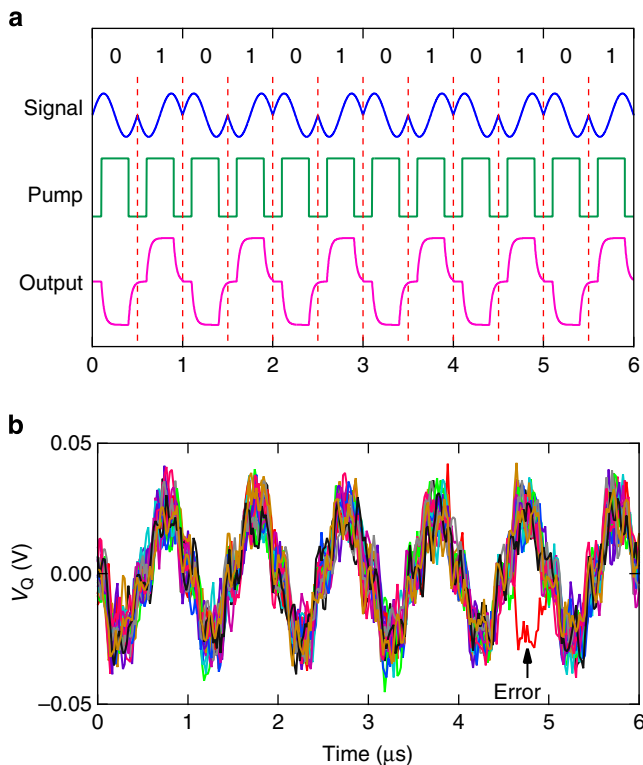
Demodulation of BPSK signal. The above result indicates the PPLO is a phase detector sensitive to very small microwave
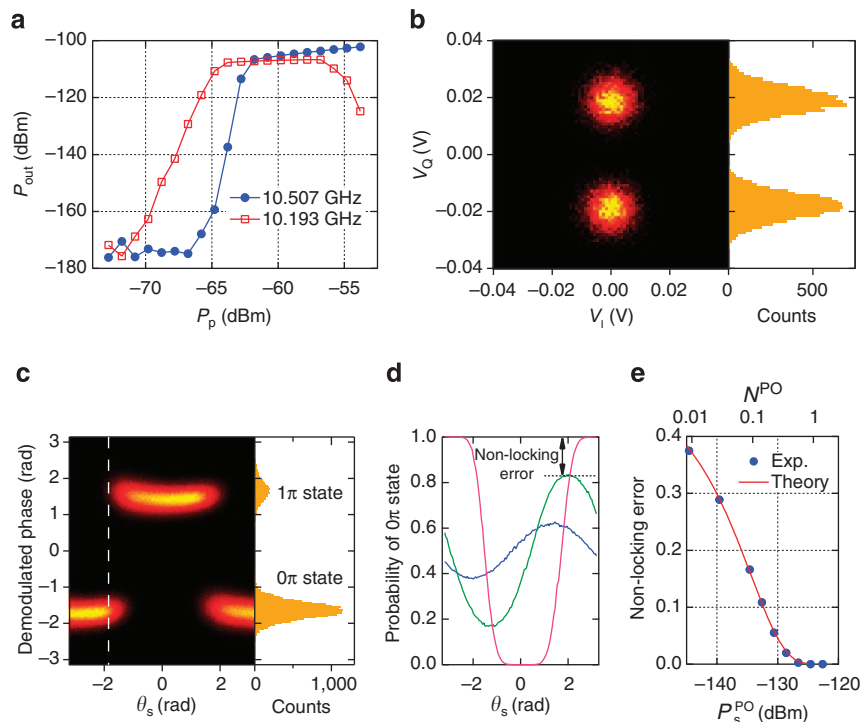
Figure 2 | Output of the PPLO. (a) Output signal power as a function of P_p at $\omega_0^{PO}/2\pi = 10.507$ GHz (solid blue circles) and $\omega_0^{PO}/2\pi = 10.193$ GHz (open red squares). The steep increase of the output power indicates onset of the parametric oscillation. For **b**–**e**, $\omega_0^{PO}/2\pi$ is set to be 10.507 GHz. **(b)** Histogram of the amplitude and phase of the output signal plotted in the quadrature (IQ) plane (left panel) and its projection onto the V_Q axis (right panel). The pulsed pump with a duration of 1.6 μs and an amplitude of -62 dBm is applied 1.6×10^4 times in total. No LS is applied. **(c)** Histogram of the output-signal phase as a function of the LS phase θ_s (left panel) and its cross-section along the dashed line (right panel). The same pulsed pump as in **b** is applied 2.0×10^4 times for each θ_s. LS is continuously applied with the power of -125 dBm. **(d)** Probability of 0π state as a function of θ_s for P_s of -145 (blue), -135 (green) and -125 dBm (magenta). Phase shifts between different curves are an artefact due to the drift of the relative phase between the two generators used for the pump and the signal. In the qubit readout measurements, we used only one generator for the pump (with a frequency doubler) and the signal to avoid this problem. **(e)** Non-locking error as a function of the LS power P_s^{PO}. Solid blue circles represent the experimental data and the red curve is the result of a simulation based on the master equation. The corresponding mean photon number in the PPLO resonator N^{PO} is plotted on the top axis.

powers of the order of a femtowatt. To demonstrate this, we generate a signal digitally modulated by BPSK, a scheme commonly used in modern telecommunications[18], and demodulate it by using a PPLO. Figure 3a shows the sequence of the experiment. The generated signal has a fixed carrier frequency of 10.503 GHz, fixed power of −125 dBm and a phase that is digitally modulated by π every 500 ns. This means that the signal carries alternating binary bits with a baseband frequency of 2 MHz. Synchronously, we apply pump pulses with the duration of 300 ns and the amplitude of −62 dBm. Figure 3b shows the superposed time traces of the PPLO output. It shows successful demodulation of the input signal except rare errors as exemplified in the figure. We sent a total of 2.4×10^4 bits and detected four errors, corresponding to the error rate of 1.7×10^{-4}. As studied in the parametron for its clock speed[19], the response time of a PPLO decreases rapidly as we increase P_p and P_s^{PO}. In the present study, we could make it comparable to the cavity decay time $(\kappa/2)^{-1}$ (see Supplementary Fig. 4). This time, together with the integration time to extract the output phase (100 ns in the present study), determines the upper limit for the baseband frequency of the BPSK signal to be demodulated, namely, the bandwidth of the PPLO as a phase detector.

Qubit readout using PPLO. Now we apply this phase discrimination capability to the dispersive readout of a qubit. Figure 4a shows the measurement set-up. A chip containing a 3-JJ superconducting flux qubit capacitively coupled to a CPW resonator (readout resonator) is connected to the PPLO via

a

circulators. The flux qubit is biased at $\Phi_q = 0.5\Phi_0$, where the qubit transition frequency from $|0\rangle$ to $|1\rangle$ states is 5.510 GHz. Figure 4b shows the phase rotation of the reflection coefficient around the resonant frequency of the readout resonator (ω_r^r) when the qubit is in $|0\rangle$ (blue) and $|1\rangle$ (green). The shift between the two curves is due to the dispersive coupling between the qubit and the readout resonator[20]. We set ω_s to be 10.193 GHz, such that the qubit states are mapped onto two phases of the reflected microwave differing by π.

We discriminate the two states by using the PPLO and the pulse sequence shown in Fig. 4a. We set $\omega_0^{PO} = \omega_s$, $\omega_p = 2\omega_s$ (corresponding to open red squares in Fig. 2a) and $P_p = -65$ dBm. Figure 4c shows the probability of detecting the 0π state as a function of the phase of the readout microwave pulse θ_s (similar to Fig. 2d) with the qubit control π pulse off (blue) and on (green). The power of the readout microwave field at the input of the readout resonator P_s^r is −120 dBm, which corresponds to the mean photon number in the readout resonator $N^r = 4P_s^r Q_L^{r\,2}/(\hbar\omega_0^{r\,2}Q_e^r) = 5.5$. Reflecting the π-phase difference of the reflected microwave field, the two curves are out of phase and their difference corresponds to the fidelity of the qubit readout, which is maximized at −2.0 and 1.2 rad to be 89%.

We further maximized the fidelity by tuning t_p and adding a short spike in the beginning of the readout pulse, and measured Rabi oscillations as shown in Fig. 4d, where the length t_c and the amplitude $\sqrt{P_c}$ of the qubit control pulse are swept. Figure 4e shows the Rabi-oscillation measurement along the dashed line in Fig. 4d. The contrast of the Rabi oscillations is 90.7%. We attribute the sources of the error to incomplete initialization of the qubit by 2.6% and to qubit energy relaxation (including the gate error of the π pulse), which adds 6.7%. Note that the non-zero minimum of the blue curve in Fig. 4c is due to incomplete initialization of the qubit and not the non-locking error. The non-locking error is confirmed to be negligible for both states of the qubit (see Supplementary Note 1 and Supplementary Figs 5 and 6 for the details).
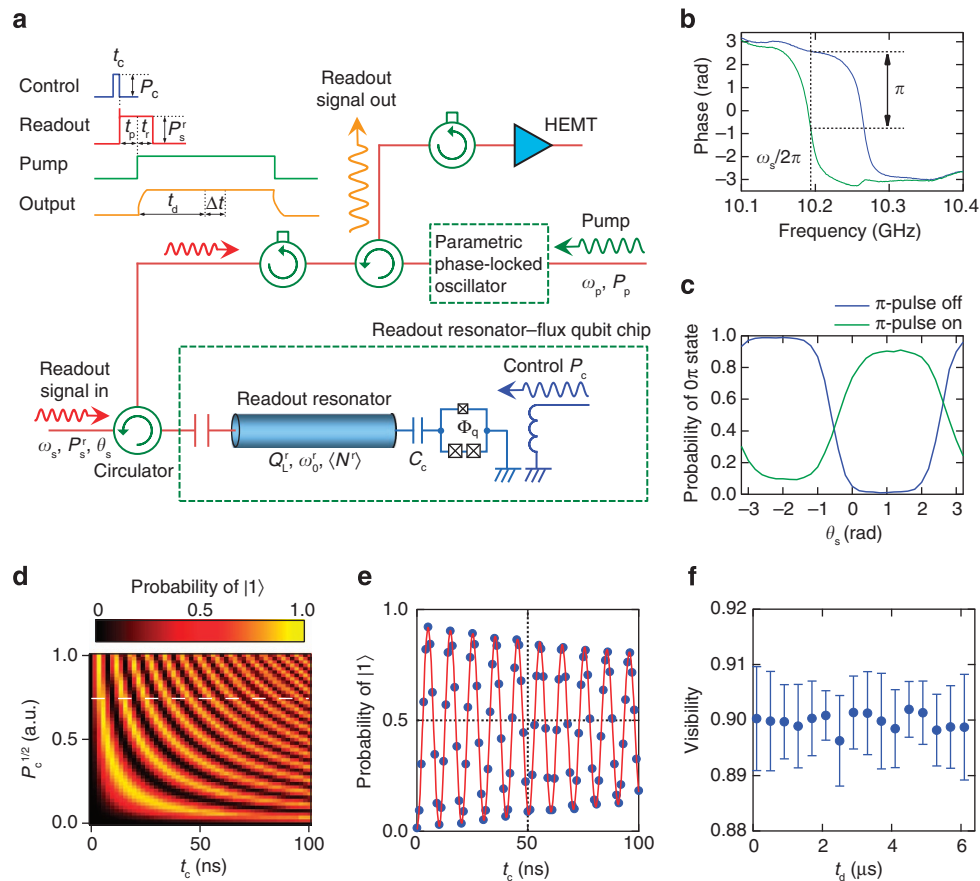
Discussion
As stated above, N^r of 5.5 is large enough to make the non-locking error of PPLO negligible. It is at the same time small enough for the qubit to avoid readout backaction. By sweeping t_p, we can measure T_1 of the qubit, while populating photons in the readout resonator. It is measured to be 690 ns (see Supplementary Fig. 7), which agrees with T_1 obtained from the independent ensemble-averaged measurement using a standard pulse sequence, namely, a π pulse followed by delayed readout. This indicates the non-destructive character of the present readout scheme.

Another characteristic of the present readout scheme is its latching property. Once the qubit state is mapped to the oscillator state of PPLO, the information can be maintained, regardless of a subsequent qubit state transition, as long as the pump is turned on. We demonstrate this in Fig. 4f, in which the readout fidelity is plotted as a function of t_d. Even at $t_d = 6\,\mu s$, at which the qubit has totally decayed, we do not lose readout fidelity.

The present scheme enables fast, latching-type and single-shot readout of the qubit. In this sense, it is similar to schemes using a Josephson bifurcation amplifier[6], Josephson-chirped amplifier[21] and period-doubling bifurcation[22], where the qubit is directly coupled to a nonlinear resonator. However, in the present scheme, the mean photon number in the resonator to which the qubit is coupled can be kept small (of order unity) regardless of the result of the readout. In this sense, it is similar to schemes where a qubit is coupled to a linear resonator, followed by an ultra-low-noise amplifier such as Josephson parametric amplifier to achieve single-shot readout[10]. Thus, the present scheme has

b

Figure 3 | Demodulation of BPSK signal. (**a**) Pulse sequence. BPSK signal at 10.503 GHz with an amplitude of −125 dBm is generated by mixing the 10.553 GHz signal and 50 MHz intermediate frequency (IF) signal (blue curve). Phase of the IF signal is digitally modulated by π (corresponding to bit '0' and bit '1') every 500 ns and the pulsed pump (green curve) is synchronously applied. The magenta curve represents the expected output of the PPLO. (**b**) Examples of the demodulated signal. Twenty individual time traces are superposed.

Figure 4 | Qubit readout using PPLO. (**a**) Measurement set-up and pulse sequence. A 3-JJ superconducting flux qubit biased at $\Phi_q = \Phi_0/2$ is capacitively ($C_c = 4$ fF) coupled to a CPW resonator. Here ω_0^r and N^r represent the resonant frequency and the mean photon number of the readout resonator, respectively. The internal (Q_i^r) and external (Q_e^r) quality factors are 2.5×10^4 and 630, respectively, resulting in the loaded quality factor Q_L^r of 620. In the pulse sequence, Δt ($= 100$ ns) represents the data acquisition time to extract the phase, and P_s^r and P_c represent the power of the readout and the qubit control pulses, respectively. A short spike was added in the readout pulse to improve the readout fidelity. In **c**–**f**, we applied the pulse sequence 1×10^4 times to obtain the probability. (**b**) Frequency dependence of the phase of the reflection coefficient of the readout resonator with qubit control π pulse on (green) and off (blue). (**c**) Probability of the PPLO 0π state as a function of the readout-signal phase θ_s with the qubit control π pulse on (green) and off (blue). Here $t_c = 10$ ns, $t_p = 50$ ns, $t_r = 50$ ns and $t_d = 300$ ns. (**d**) Rabi oscillations measured with $t_p = 30$ ns, $t_r = 50$ ns and $t_d = 300$ ns. (**e**) Rabi oscillations along the dashed line in **d**. Red curve represents a fit with an exponentially damped sinusoidal function. (**f**) Visibility as a function of t_d. Here $t_c = 10$ ns, $t_p = 30$ ns and $t_r = 50$ ns. The error bars represents the standard deviation in five identical measurements.

combined advantages of both linear and nonlinear resonators and can be useful in quantum error-correction protocols such as the surface code[23].

References

1. Onyshkevych, L. S., Kosonocky, W. F. & Lo, A. W. Parametric phase-locked oscillator–characteristics and applications to digital systems. *Trans. Inst. Radio Engrs.* **EC-8,** 277–286 (1959).
2. Goto, E. The parametron, a digital computing element which utilizes parametric oscillation. *Proc. Inst. Radio Engrs.* **47,** 1304–1316 (1959).
3. Mahboob, I. & Yamaguchi, H. Bit storage and bit flip operations in an electromechanical oscillator. *Nat. Nanotechnol.* **3,** 275–279 (2008).
4. Wang, Z., Marandi, A., Wen, K., Byer, R. L. & Yamamoto, Y. Coherent Ising machine based on degenerate optical parametric oscillators. *Phys. Rev. A* **88,** 063853 (2013).
5. Dykman, M. I. (ed.) *Fluctuating Nonlinear Oscillators: From Nanomechanics to Quantum Superconducting Circuits* (Oxford University Press, 2012).
6. Siddiqi, I. et al. Dispersive measurements of superconducting qubit coherence with a fast latching readout. *Phys. Rev. B* **73,** 054510 (2006).
7. Vijay, R., Slichter, D. H. & Siddiqi, I. Observation of quantum jumps in a superconducting artificial atom. *Phys. Rev. Lett.* **106,** 110502 (2011).
8. Wallquist, M., Shumeiko, V. S. & Wendin, G. Selective coupling of superconducting charge qubits mediated by a tunable stripline cavity. *Phys. Rev. B* **74,** 224506 (2006).
9. Yamamoto, T. et al. Flux-driven Josephson parametric amplifier. *Appl. Phys. Lett.* **93,** 042510 (2008).
10. Lin, Z. R. et al. Single-shot readout of a superconducting flux qubit with a flux-driven Josephson parametric amplifier. *Appl. Phys. Lett.* **103,** 132602 (2013).
11. Wilson, C. M. et al. Photon generation in an electromagnetic cavity with a time-dependent boundary. *Phys. Rev. Lett.* **105,** 233907 (2010).
12. Krantz, P. et al. Investigation of nonlinear effects in Josephson parametric oscillators used in circuit quantum electrodynamics. *New J. Phys.* **15,** 105002 (2013).
13. Ryvkine, D. & Dykman, M. I. Resonant symmetry lifting in a parametrically modulated oscillator. *Phys. Rev. E* **74,** 061118 (2006).
14. Kim, Y. et al. Observation of resonant symmetry lifting by an effective bias field in a parametrically modulated atomic trap. *Phys. Rev. A* **82,** 063407 (2010).
15. Mahboob, I., Froitier, C. & Yamaguchi, H. A symmetry-breaking electromechanical detector. *Appl. Phys. Lett.* **96,** 213103 (2010).
16. Dykman, M. I., Maloney, C. M., Smelyanskiy, V. N. & Silverstein, M. Fluctuational phase-flip transitions in parametrically driven oscillators. *Phys. Rev. E* **57,** 5202–5212 (1998).
17. Johansson, J., Nation, P. & Nori, F. Qutip 2: a Python framework for the dynamics of open quantum systems. *Comput. Phys. Commun.* **184,** 1234–1240 (2013).
18. Anderson, J. B., Aulin, T. & Sundberg, C.-E. *Digital Phase Modulation* (Plenum, 1986).
19. Beer, K. W. An experimental investigation into the operation of the parametric phase-locked oscillator. *Radio Electron. Eng.* **25,** 432–440 (1963).

20. Inomata, K., Yamamoto, T., Billangeon, P.-M., Nakamura, Y. & Tsai, J. S. Large dispersive shift of cavity resonance induced by a superconducting flux qubit in the straddling regime. *Phys. Rev. B* **86,** 140508 (2012).
21. Naaman, O., Aumentado, J., Friedland, L., Wurtele, J. S. & Siddiqi, I. Phase-locking transition in a chirped superconducting Josephson resonator. *Phys. Rev. Lett.* **101,** 117005 (2008).
22. Zorin, A. B. & Makhlin, Y. Period-doubling bifurcation readout for a Josephson qubit. *Phys. Rev. B* **83,** 224506 (2011).
23. Fowler, A. G., Mariantoni, M., Martinis, J. M. & Cleland, A. N. Surface codes: Towards practical large-scale quantum computation. *Phys. Rev. A* **86,** 032324 (2012).

Acknowledgements

Author contributions

T.Y. and Z.R.L. conceived the experiment and wrote the manuscript. Z.R.L. performed the measurement and analysed the data. K.I. fabricated the qubit device and helped with the measurement and analysis. T.Y. designed PPLO, which was fabricated at the group of W.D.O. K.K. and T.Y. developed the theory and performed the numerical simulations. All authors contributed to the discussion of the results and helped in editing the manuscript.

Additional information